Research Article | Vol. 27, No. 6 | 18 Mar 2019 | OPTICS EXPRESS 8696

Optics EXPRESS

Low loss optical waveguides fabricated in $LiTaO_3$ by swift heavy ion irradiation

V. TORMO-MARQUEZ,[1] M. DÍAZ-HIJAR,[1,2] M. CARRASCOSA,[3] V. YA. SHUR,[4] AND J. OLIVARES[1,2,*]

[1]*Centro de Microanálisis de Materiales (CMAM), Universidad Autónoma de Madrid (UAM), 28049 Madrid, Spain*
[2]*Instituto de Optica, Consejo Superior de Investigaciones Científicas, (IO, CSIC), C/Serrano 121, 28006 Madrid, Spain*
[3]*Dpto. Física de Materiales, Universidad Autónoma de Madrid (UAM), 28049 Madrid, Spain*
[4]*School of Natural Sciences and Mathematics, Ural Federal University, 620000 Ekaterinburg, Russia*
[*]*jose.olivares@csic.es*

Abstract: Optical waveguides are fabricated by irradiation of $LiTaO_3$ with a variety of swift heavy ions that provide increasing levels of both nuclear and electronic damage rates, including C, F and Si ions, in the energy range of 15-40 MeV. A systematic study of the role of the ion fluence has been carried out in the broad range of 1e13-2e15 at/cm^2. The kinetics of damage is initially of nuclear origin for the lowest fluences and stopping powers and, then, is enhanced by the electronic excitation (for F and Si ions) in synergy with the nuclear damage. Applying suitable annealing treatments, optical propagation losses values as low as 0.1 dB have been achieved. The damage rates found in $LiTaO_3$ have been compared with those known for the reference $LiNbO_3$ and discussed in the context of the thermal spike model.

1. Introduction

Lithium tantalate ($LiTaO_3$: LT) and lithium niobate ($LiNbO_3$: LN) are among the most important materials used in the last decades for integrated photonic applications given their ferroelectric, optoelectronic and nonlinear optical properties [1]. Initially, the fact that the Curie temperature of $LiTaO_3$ (T_c ~615-695 °C) is lower than the temperatures needed for the fabrication of optical waveguides by ion diffusion (typically above 1000 °C) favoured the use of $LiNbO_3$ for the initial progress of the integrated optics technology. The development of integrated devices based on the high nonlinear optical coefficients, like laser frequency conversion, is a particular field that has grown steadily and has maintained a high interest up to nowadays [2]. For these kind of applications LiTaO3 offers some clear advantages compared to $LiNbO_3$ like a higher photorefractive damage resistance and a wider optical transmission range in the UV [3–5]. For fostering nonlinear optical applications a great development took place in the topic of ferroelectric domain reversal, particularly for quasi phase matching (QPM) second harmonic generation (SHG) [6–9]. This so called "ferroelectric domain engineering" has, in turn, promoted further avenues for novel material patterning and structuring by exploiting the differential domain etching rate. It is worth to remark the superior capability of LT crystals to allow for smaller domain patterning than LN crystals, making easier the fabrication of submicron size domain patterns [7].

Optical waveguide fabrication techniques using temperatures lower than Tc, like proton-exchange (PE), have succeeded in using $LiTaO_3$ preserving the desired ferroelectric domain structure relevant for the device operation [10,11]. Ion implantation has been shown to be a good technique for optical waveguide fabrication for many materials. Initially, light ion (i.e. H or He) implantation with a few MeV energy was mostly used, exploiting the structural (nuclear) damage caused by the elastic collisions at the end of the ion range. The buried damaged layer typically has lower density and lower refractive index, creating an optical

#356013 https://doi.org/10.1364/OE.27.008696
Journal © 2019 Received 26 Dec 2018; accepted 3 Feb 2019; published 11 Mar 2019

Optics EXPRESS

barrier that builds the optical waveguide under the surface [12]. Some specific studies were reported in LT crystals [13–15]. However, the fluences needed for good optical confinement using light ion implantation are very high, of the order of 10^{16}-10^{17} at/cm^2. Interestingly, the use of buried damaged layers produced by ion implantation have been found to be good for producing easier, better and smaller domain reversal patterning in LN with nanometer sizes [16–18]

Recently, the use of irradiations with heavier ions (i.e. A > 10) at higher energies (≥ 1 MeV/amu, also called swift heavy ions or SHI) such that the maximum electronic energy loss (or stopping power, Se) takes place some microns underneath the surface, has been proposed for fabricating good and novel optical waveguides in $LiNbO_3$ [19–21] and other oxides [22,23] with the pragmatic benefit of using fluences several orders of magnitude lower than those used with light ion implantation. The defects and damage generation of SHI and the final structural changes that cause the useful refractive index modification are strongly related to the high electronic energy density deposited along the ions tracks. It is, then, referred as electronic damage as compared to the nuclear damage occurring mostly at the end of the ion tracks and not being, in principle, very relevant in this method. Several regimes of damage creation and accumulation have been studied in LN. For medium mass ions (like F) moderate damage is created per ion track that accumulates, after track overlapping given enough fluence, to finally create buried thick amorphous layers with sharp boundaries and high refractive index change (decrease >10%) that allows for high optical confinement [19,20]. This method of waveguide fabrication has been applied for the fabrication of demanding devices like micro-rings resonators [24] or in innovative applications such as nanoparticle trapping and patterning [25]. The capability to preserve periodic ferroelectric domain patterns has also been ascertained [26]. On the high energy loss regime, using much heavier ions, the energy loss per ion track increases above the so called amorphization threshold (Se,th, characteristic of each material, being around 6 keV/nm for LN); each ion creates along its trajectory an amorphous latent track, whose diameter (a few nm) is proportional to the energy loss and, therefore, is increasing along the track following the energy loss curve. This type of high energy irradiation creates, by keeping the fluence in the isolated track regime (i.e. at ultralow fluences of the order of 1011 at/cm2), an effective nanostructured medium that behaves like an optical waveguide. It can be quite thick (10´s of µm) and useful for good waveguiding of long wavelength infrared light [27,28]. Being clear that the electronic energy deposition of SHI plays a fundamental role in the damage generation and the subsequent structural changes of the diverse irradiated materials, the rigorous modeling and understanding of the basic mechanisms of the damage process are still under debate in the community, as discussed in several reviews [29,30].

Given the great interest in the potential combination of the several excellent optical and ferroelectric properties of LiTaO3 with the potential of SHI irradiation structuring, we have considered to study systematically the fabrication and characterization of optical waveguides in $LiTaO_3$ by means of using swift heavy ion irradiation. Aside from the interest in potential technological achievements, taking as a reference the broad knowledge available in the close material $LiNbO_3$ can strongly help to improve the understanding of the fundamental aspect of SHI damage generation. There are very scarce data published on this subject, even showing contradictory results in the damage mechanism for a case with C irradiation [31,32], just using one fluence for a case of heavier Ar ion [33] and all reporting higher propagation losses than we report here. We have explored a more systematic set of experimental conditions, regarding the key parameters under SHI irradiation, the value of Se (keV/nm), varied using C, F and Si ions, and the fluencies.

2. Waveguide fabrication by swift ion irradiation

Z-cut 1 mol% MgO doped stoichiometric LiTaO3 plates (SLT) were provided by Oxide Corporation, Japan, and Z-cut congruent LiTaO3 wafers (CLT) from Roditi Corporation. The

Optics EXPRESS

samples thickness is 1mm and most of the samples were cut in pieces of about 5x5 mm for the systematic irradiations and subsequent characterization. Some of the samples were cut with longer lengths, of 10-20 mm, so as to facilitate optical propagation losses measurements. The samples were irradiated, in the 5 MV tandetron accelerator at the CMAM [34], with C, F and Si ions at various high energies in the 15-40 MeV range for waveguide fabrication. Some low energy irradiations (at 300-500 keV) were made in order to place the nuclear damage near the surface to make it accessible for complementary characterization by optical reflectance measurements. Two beamlines of the CMAM were used along this project: the "standard" beamline (STD) were the homogeneous beam size is 6x6 mm, and the "implantation" beamline (IMP) were the mm-size beam is electrostatically scanned (at kHz's frequencies) in the horizontal and vertical axis so as to cover homogenously irradiation areas of several cm^2. By default, the samples were tilted 5° relative to normal ion incidence to avoid channeling. Some set of samples were irradiated in the STD beamline at 45° angle of incidence for practical purposes to enlarge the irradiated length a few mm's to allow to fabricate longer waveguides. The ion beam current density was kept below 200 nA/cm^2 to minimize charging and heating of the samples. With a thermal imaging camera we could check that the surface temperature is kept within a reasonable range (<100 °C) that avoids significant defect annealing, which typically requires higher temperatures, as discussed later in this work.

Our initial strategy to select the type of ion irradiation, with the aim of efficient waveguide fabrication, takes into account as a reference the detailed information available from waveguide fabrication and ion track formation in the close material $LiNbO_3$, as presented in the introduction section. Irradiation of LN with fluorine ions in the range of 20 MeV energy produces the desired thick buried damaged layers due to the electronic excitation, and using moderate ion fluences of the order of 10^{14} at/cm^2. On the other hand, above a threshold in the stopping power ($S_{e,th}$) of around 6 keV/nm (ion velocity dependent), amorphous tracks are formed for each ion impact, since the energy density deposited is enough to cause melting (and subsequent ultrafast quenching) [29]. In this regime, an excessive (still low) ion fluence causes amorphization up to the surface, preventing the waveguide formation. Unfortunately, in the case of LiTaO3, the value of the amorphization threshold for amorphous track formation has not been ascertained yet. The analysis based on thermal-spike models is recognized as valid in such high energy (melting) regime. The phenomenological model of Szenes [35] is particularly useful to obtain some estimations, since the maximum temperature increase in the track is given by: $\Delta T = A \cdot S_e /(\rho \cdot C)$, ρ being the density and C the specific heat, and A is a factor that has been studied to take similar values for similar insulators. The Table 1 collects the main parameters relevant for a thermal spike for LN and LT.

Table 1. Main parameters relevant for a thermal spike model for LN and LT.

	$LiNbO_3$	LiTaO3
ρ (g/cm^3)	4.64	7.46
C (J/g·K)	0.63	0.42
T_m (°C)	1255	1650
$\Delta T_{LT} / \Delta T_{LN}$	$= (\rho_{LN} \cdot C_{LN}) / (\rho_{LT} \cdot C_{LT}) = 0.93$	

The Fig. 1 shows the evolution of the stopping power as a function of depth, calculated with SRIM-2013 [36], for all the cases studied in this work. For the case of F irradiation we also show as a reference the data for LN (i.e. F 20 MeV, dotted line). The maximum values of S_e for LN and LT are nearly the same (about 3.5 keV/nm). The estimated temperature increase in the spike is close for LT as compared to LN (actually, a factor 0.93 lower). Since the melting temperature of LT is significantly higher than LN, one should expect that F irradiations will not induce excessive damage, compared to LN data, since we should be well below the threshold for track formation. In fact, the estimated amorphization threshold ($S_{e,th}$)

Optics EXPRESS

for LT, referenced to the one of LN, would be simply given by (T_i being the irradiation temperature):

$$\frac{S_{e,th}^{LT}}{S_{e,th}^{LN}} = \frac{_{LT}\cdot C_{LT}}{_{LN}\cdot C_{LN}} \frac{(T_m^{LT} - T_i)}{(T_m^{LN} - T_i)} \approx \frac{_{LT}\cdot C_{LT}}{_{LN}\cdot C_{LN}} \frac{(T_m^{LT})}{(T_m^{LN})} \approx 1.4 \quad (1)$$

Then, using an amorphization threshold for LN of about 6 keV/nm, the one for LT would be: 8.4 keV/nm, which is above all the stopping powers used in this work.

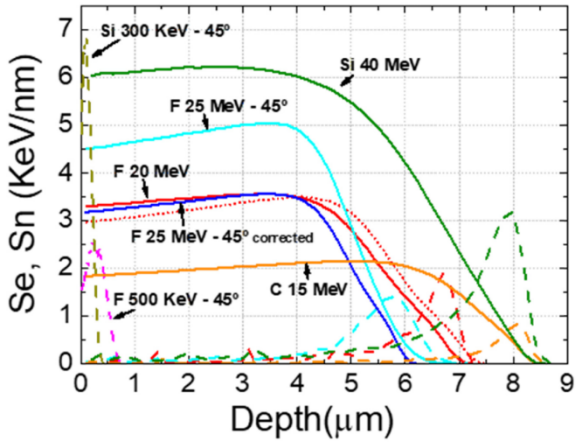

Fig. 1. Electronic (S_e, solid lines) and nuclear (S_n, dashed lines, multiplied by a factor 10 for clarity) stopping powers curves as a function of penetration depth, calculated from SRIM-2013, for the different ions used in this study on LiTaO3, as indicated with labels in the figure. The electronic stopping power curve for F 20 MeV ions on $LiNbO_3$ is also included (dotted line) for comparison as discussed in the text. The Se curve labeled "F 25 MeV-45° corrected" has been prepared using the SRIM data for F 25 MeV at normal angle of incidence and then compressing the depth scale to allow for the angle projection, so as to keep considering the real linear energy density along the ion track, that is the relevant value in a thermal spike model, as discussed in the text. We also present (for comparison and discussion) the direct SRIM output for F25 MeV at 45° which shows a larger Se value than at normal incidence, due to the type of calculation that averages the total ion energy in the thinner projected irradiated layer.

3. Waveguide characterization

The waveguide modes have been characterized by the prism coupling dark m-lines technique, using a 5 mW He–Ne laser (wavelength = 632.8 nm). From the measured set of effective refractive indices of the modes and/or resonances [12], the refractive index profile is determined using the IWKB algorithm [37]. Optical propagation losses were determined using the longest samples, by measuring the scattered laser light along the beam trajectory in the waveguide with a CCD camera. Annealing at several temperatures were performed in a tubular furnace in air atmosphere to remove irradiation color and scattering centers.

Some complementary in situ optical reflectance measurements were performed during the irradiation of some samples using low energy ion (F 500 keV and Si 300 keV). These irradiations were made at 45° incidence angle so as to facilitate that the optical reflection measurement is made at near normal incidence of the sample, using an optical port placed at 45° in the vacuum irradiation chamber. From this optical reflectance, the surface refractive index is estimated using the Fresnel relation. We used an unpolarized white light source and therefore, being the substrates z-cut oriented, the ordinary refractive index is probed. This technique is presented in more detail in Ref [38]. The aim here is to place at the surface a similar value of the nuclear stopping power than the one that is buried when using the high energies that form waveguides.

Optics EXPRESS

In order to characterize the structural disorder induced in the irradiated samples, along the first few microns underneath the surface, Rutherford Backscattering experiments in channeling configuration (RBS/c) were performed, along the c-axis channel, using H ions at 3 MeV.

4. Optical waveguides with fluorine irradiations

4.1 F 25 MeV at 45° angle incidence on stoichiometric LiTaO3

The Fig. 2 shows the results for the irradiations of SLT crystals made with F 25 MeV ions at 45° angle of incidence. It shows the measured dark mode effective indices (left side) and their corresponding refractive index profiles determined (right side) for the ordinary (top) and the extraordinary (bottom) polarizations.

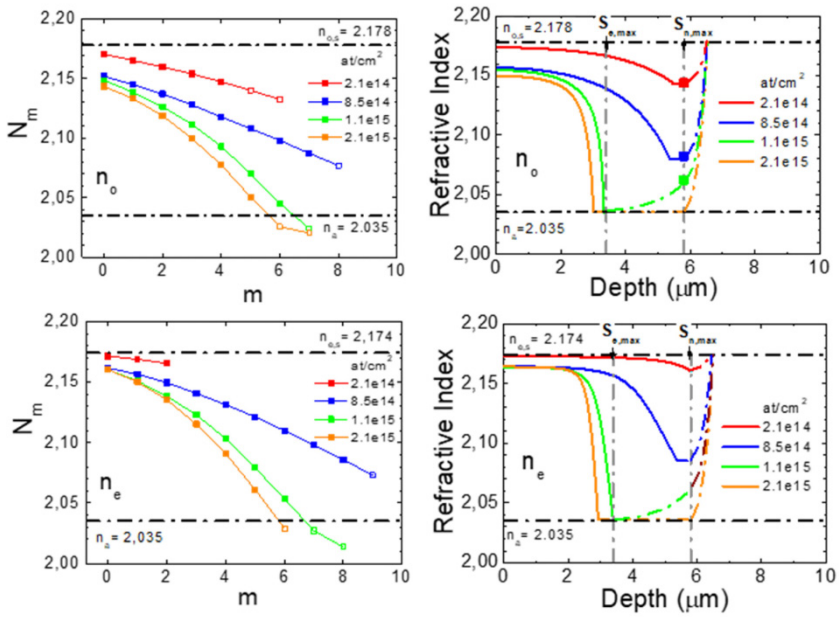

Fig. 2. Measured (λ = 632.8 nm) dark modes effective refractive indices (Nm, left side) and their corresponding refractive index profiles (right side, solid lines) for the ordinary (top) and extraordinary (bottom) polarizations, for the SLT samples irradiated with F25 MeV ions at 45° incidence angle, at the fluences indicated in the figure. The dashed lines part of the refractive index profiles are just guesses that are consistent with the nuclear stopping power curves. The refractive indices corresponding to the virgin substrate ($n_{o,s}$ and $n_{e,s}$) and to the amorphous state (n_a = 2.035) are shown with horizontal dashed lines for reference. The depth positions for both, the maximum electronic and nuclear stopping power curves (Fig. 1), are shown with vertical dashed lines. The symbols correspond to data obtained from the optical reflectance measurement (only ordinary polarization) using the low energy ion irradiation for reference, as discussed in the text.

We see that, for the lowest fluences necessary to produce some refractive index change to allow for some guided modes, in the order of $2x10^{14}$ at/cm^2, the refractive index profiles are proportional to the nuclear stopping power curve, showing the maximum value at a depth of about 5.8 μm. Already this results can be compared to those in the reference material LN, where for the same fluences, a thick amorphous layer is formed due to the electronic damage, as discussed in detail in the literature [19,30]. For a higher fluence of $8.5x10^{14}$ at/cm^2 (i.e. a factor 4 higher) the maximum of the damage (i.e. minimum refractive index) is slightly shifted towards a shorter depth. It also shows a small decrease along all the refractive index profile up to the surface. Interestingly, for just a bit higher (x1.2) fluence of $1.1x10^{15}$ at/cm^2, the minimum refractive index has moved several microns, to about the same position where

Optics EXPRESS

the maximum value of S_e is placed (at 3.6 μm). Moreover the minimum refractive index corresponds with the amorphous value and, in addition, we already get a quite sharp refractive index profile, similar to those reported for LN. Doubling (approximately) the last fluence up to 2.1×10^{15} at/cm^2 further causes the sharp boundary to slightly move towards a smaller depth as also happens for LN [19]. The refractive index of the amorphous state ($n_a = 2.035$), shown in Fig. 2 for reference, is a relevant parameter for the optical waveguides characterization and the underlying damage analysis, that has been obtained more accurately from the combined analysis of all the refractive indices profiles studied shown in this work for all the ions.

4.2 Damage assessment by RBS/C data

In Fig. 3 we show the characterization, using RBS/channeling, of the disorder induced in the first few microns underneath the surface by the same ion irradiations discussed in the previous section (with the refractive index profiles shown in Fig. 2).

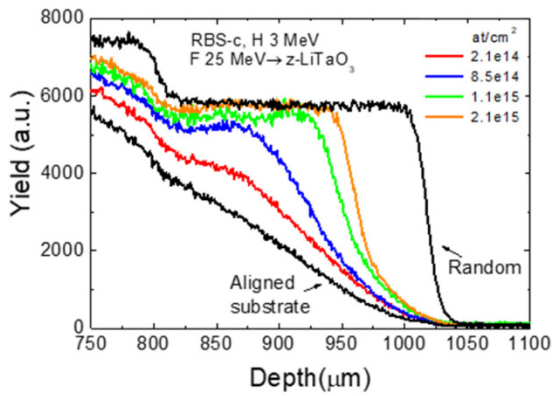

Fig. 3. RBS/channeling spectra measured along the c axis with H 3 MeV particles on z-cut stoichiometric LiTaO3 irradiated with F 25 MeV ions at 45° incidence angle, with several fluences indicated in the figure. The spectra of a virgin sample is also shown in both channeling and random configurations. The abscissa axis of the measured spectra (energy channel) has been converted to depth to allow for comparison with the corresponding refractive index profiles shown in Fig. 2.

Several valuable pieces of information can be obtained from the RBS-c spectra. First thing to be remarked is the good crystallinity shown by the irradiated crystal in the near surface region (i.e. in the first micron). Therefore, the small but significant decrease of refractive indices measured at the surface (Fig. 2) is not directly associated to standard "damage" but it might be related to some macroscopic effect related to the induced strain and stress, subject studied with TEM analysis in low energy implantations of LT [39]. On the other hand, the depths at which the maximum damage occur can be compared to those obtained from the refractive index profiles (Fig. 2) showing good agreement. Indeed, we clearly see, for the fluence of 1.1×10^{15} at/cm^2 the transition from the pure nuclear damage regime to the case where the electronic stopping power is playing a significant additional or synergetic role. Interestingly, at that fluence, we can still appreciate two distinct maximum disorder peaks (at about 5.8 and 3.4 μm) that can be nicely correlated with both maximum of the nuclear and electronic stopping power curves, respectively. For the highest fluence studied already a full flat disordered layer is observed. Here, is timely to comment on the measurements made by optical reflectance during irradiation with low energy ions (F 500 KeV and Si 300 keV). The value of the nuclear stopping power at the surface is close to the maximum values that are placed deep for high energy as shown in the SRIM calculations of Fig. 1. From the reflectance signal we determine, using the Fresnel relation, the equivalent (fluence-like) ordinary refractive indices shown with symbols in Fig. 2 (top, right) as a reference. We, then, emphasize that although is not a direct measurement on such specific waveguides, it can be

Optics EXPRESS

considered a valuable data since the dark mode analysis give no accurate information of the back side of the optical barrier. It can be observed that for the transition fluence of $1.1x10^{15}$ at/cm^2 the full amorphization has not been achieved at the maximum of the nuclear stopping power curve.

4.3 F 20 MeV on congruent LiTaO3

We also performed irradiations with F 20 MeV ions at quasi-normal incidence (about 5° incidence) at various fluences in CLT. We chose this configuration as the default one so as to use our IMP beamline and benefit of large irradiation area and in futures works of some extra equipments installed there. In Fig. 4 we show the measured effective refractive indices and their corresponding refractive index profiles. We also show the results after some low temperature annealings performed to study the optimization of the propagation losses, later discussed.

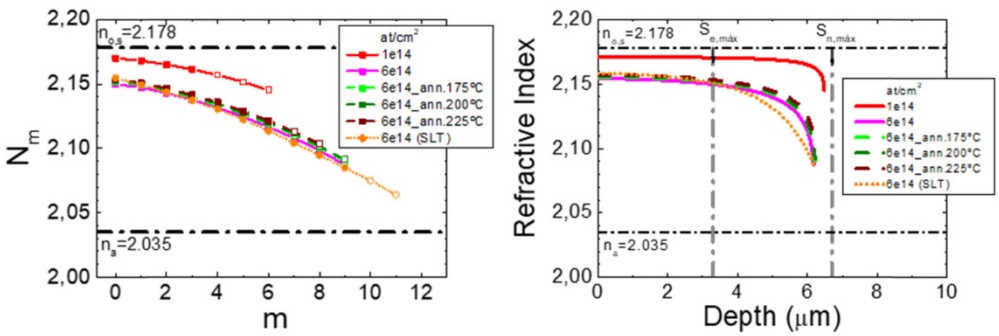

Fig. 4. Measured (λ = 632.8 nm) dark modes effective refractive indices (N_m, left side) and their corresponding refractive index profiles for the ordinary polarization, for the CLT samples irradiated with F 20 MeV ions, at the fluences indicated in the figure. The depth positions for both, the maximum electronic and nuclear stopping power curves (see Fig. 1), are shown with vertical dashed lines.

The initial stages of damage seems to appear at the same order of magnitude of fluence of about $1x10^{14}$ at/cm^2 and, as a general trend, also following the nuclear stopping power curve that has its maximum at a depth of 6.7 μm. However, a difference in the refractive index profile shape can be appreciated, being now less gradual from the surface (or being more step-like), even up to the intermediate fluence of $6x10^{14}$ at/cm^2. It must be remarked that the depth position of the maximum of S_n is now significantly separated from maximum of the S_e curve, as can be appreciated both in the SRIM data of Fig. 1 and with the corresponding reference vertical dashed lines in Figs. 2 and Fig. 4. This support the hypothesis of the possible synergy effects in the cross section for damage generation. After some seed of accumulated nuclear damage at the end of the ions range, the electronic excitation of subsequent ion tracks reaching the inner boundary of such predamaged regions, shows and effective lower threshold for enhancing further damage. Recently, such phenomena of synergy between the electronic excitation and the nuclear damage is being studied in various materials and specifically in LT [40].

With the results presented so far with fluorine ions we can ascertain that the estimation made with the thermal spike model for our irradiation strategy has been good to explore a range of fluence that allow to produce waveguides showing from gradual refractive indices profiles to step-like ones. For expanding this investigation in the main parameters for potential tuning the fabrication capabilities (the values of S_e and S_n), we decide to explore both, lighter (i.e., C) and heavier ion (i.e. Si). For the case of a lighter ion, we choose C irradiations so as to compare to reported contradictory results [31,32].

Optics EXPRESS

5. Optical waveguides with carbon irradiations

Figure 5 shows the ordinary refractive index profiles obtained for irradiations of CLT with C 15 MeV ions at three fluences. All the profiles are closely proportional to the corresponding S_n curve. For the same fluence range than in F irradiations, the damage as seen by the refractive index change is smaller, and roughly proportional, as it should be, to the lower mass and lower values of S_n shown in Fig. 1. For the highest fluence of $1x10^{15}$ at/cm^2 the maximum refractive index change is not higher than about 50%. In this same fluence range are the data of ref [31]. using a lower energy (6 MeV) that are in agreement with this work, and the data of ref [32]. using the same energy (15 MeV, fluence $2x10^{14}$ at/cm^2) that are not in agreement with this work. From our point of view a possible explanation that could explain the "higher" electronic damage seen in ref [31], could be that they had significant heating of the sample during irradiation, in which case, according the thermal spike model already commented, the effective threshold for electronic damage generation is lower.

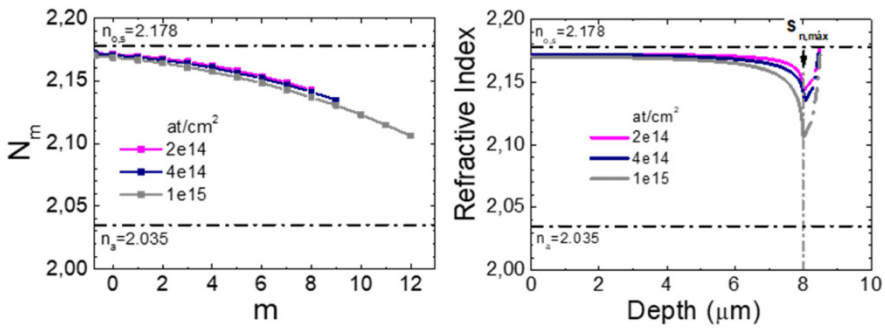

Fig. 5. Measured (λ = 632.8 nm) dark modes effective refractive indices (N_m, left side) and their corresponding refractive index profiles for the ordinary polarization, for the CLT samples irradiated with C 15 MeV ions, at the fluences indicated in the figure. The depth positions for the maximum nuclear stopping power curve (see Fig. 1), is shown with vertical dashed line.

6. Optical waveguides with silicon irradiations

6.1 Si 40 MeV on congruent LiTaO3

The Fig. 6 shows the results for the irradiations of CLT crystals made with Si 40 MeV ions. It shows the measured dark mode effective indices (left side) and their corresponding refractive index profiles determined (right side) for both polarizations. For the lowest fluences that produce only one or two measured dark modes an accurate refractive index profile cannot be produced. Nevertheless, from the effective mode values and their slope (for the case of two modes) some rough profile shapes can be guessed. It can be estimated (lowest fluences, 2 modes) and seen that the maximum damage is firstly located deep, near the depth of $S_{n,max}$ and then "shifts" progressively towards the depth at which is located the maximum of S_e. The complementary data obtained from the in situ optical reflectance (symbols) show again, and in this case even more clearly, the different rate of damage generation when comparing the pure effects of S_n with the combined or synergetic effects of S_e and S_n. We obtain significant damage for much lower fluences than for the F irradiations, about one order of magnitude lower.

Optics EXPRESS

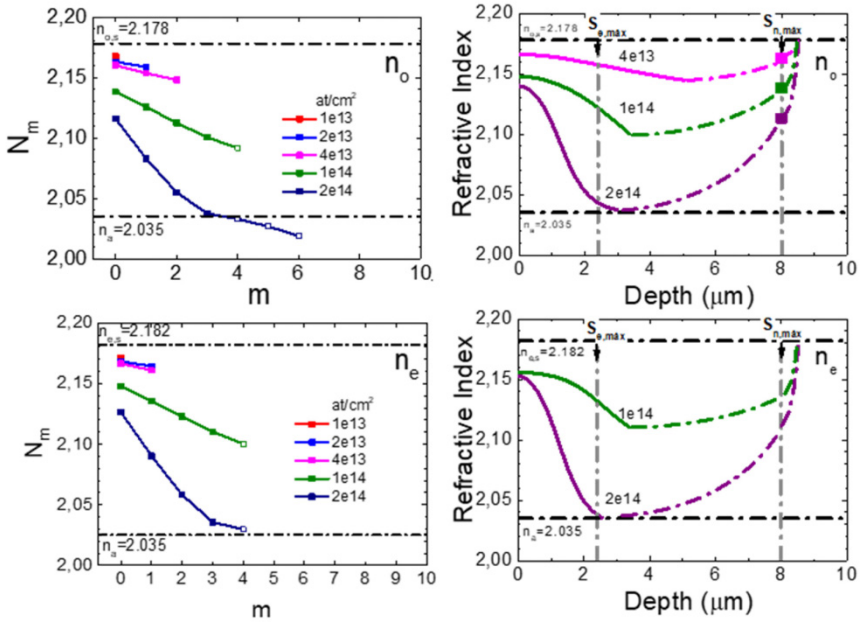

Fig. 6. Measured (λ = 632.8 nm) dark modes effective refractive indices (N_m, left side) and their corresponding refractive index profiles (right side, solid lines) for the ordinary (top) and extraordinary (bottom) polarizations, for the CLT samples irradiated with Si 40 MeV ions, at the fluences indicated in the figure. The dashed lines part of the refractive index profiles are just guess that are consistent with the nuclear stopping power curves. The depth positions for both, the maximum electronic and nuclear stopping power curves (Fig. 1), are shown with vertical dashed lines. The symbols correspond to data obtained from the optical reflectance measurement (only ordinary polarization) using the low energy ion irradiation for reference, as discussed in the text.

Nevertheless, the fluence is still high enough to claim that we are in the track overlapping regime (corresponding the isolated track regime to fluences up to some $5x10^{11}$ at/cm^2). Our results show that we are, therefore, below the amorphization threshold with the electronic stopping values of the Si irradiation. This is consistent with the estimation we made in Section 3, using the thermal spike model, for the latent track formation threshold for LT being about 8.4 keV/nm. Is worth here to comment that in the work of ref [33]. the authors use swift Ar irradiation that has a maximum value of S_e of just 8.3 keV/nm. For the low fluence they used of $2x10^{12}$ at/cm^2, track overlap is still not very high and, therefore, the damage generated is also low, as they found.

6.2 Damage assessment by RBS/C data

In Fig. 7 we show the characterization, using RBS/channeling, of the disorder induced in the first few microns underneath the surface by the same ion irradiations discussed in the previous section (with the refractive index profiles shown in Fig. 6).

Optics EXPRESS

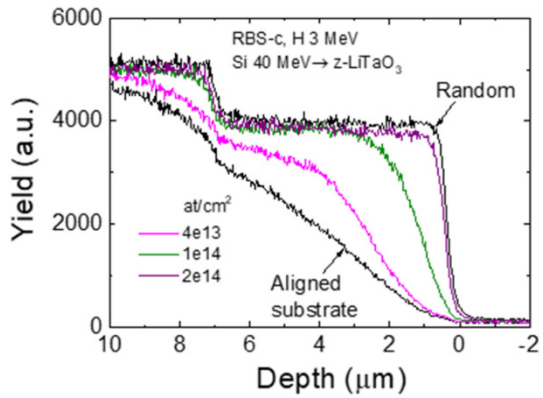

Fig. 7. RBS/channeling spectra measured along the c axis with H 3 MeV particles on z-cut CLT irradiated with Si 40 MeV ions, with several fluences indicated in the figure. The spectra of a virgin sample is also shown in both channeling and random configurations. The abscissa axis of the measured spectra (energy channel) has been converted to depth to allow for comparison with the corresponding refractive index profiles shown in Fig. 6.

7. Optimization of optical propagation losses

The optical waveguides fabricated by ion irradiation (in most dielectrics) show high optical propagation losses, mainly due to color centers causing absorption bands and also due to some scattering centers as a result of local stressed regions. We have performed several sequential steps of annealing (1h each step, in air) at increasing temperatures (175, 200, 225 °C) to some of the waveguides made by F and Si irradiations and whose refractive index profiles have been shown in previous sections. In Fig. 8 we show, as an example, the propagation losses image and its corresponding analysis for the case of irradiation of CLT with F 20 MeV and annealed up to 225 °C showing a very good value as low as 0.8 dB/cm. In Fig. 8 we show the best values obtained, for the moment in this on-going work, for reasonably high optical confinement (i.e., high refractive index change). We achieve propagation losses under 0.5 dB/cm for both type of ions, F and Si. We remark here that we have ascertained that theses low temperature annealings preserve the refractive index profiles, as is shown in Fig. 5 for the case of F 20 MeV irradiation. We note that our propagation losses are better than those reported in the two references using SHI already commented [32,33].

Obviously, one of the desired objectives would be to have low propagation losses for any of the possible waveguides fabricated and, particularly, for those showing the highest optical confinement, i.e. step-like refractive index profiles. Unfortunately, we have found at this stage the somehow surprising result that, increasing the annealing temperature above some 250-300 °C, produces worse results, due to the appearance of some cracks, probable due to the relaxation of accumulated strains. This does not happens in the equivalent LN waveguides produced by F ion irradiation where annealing in the range 300-350 °C still reduced optical losses [19,20]. It is timely to cite here various works on damage induced in LT by low energy Ar implantation (i.e. nuclear damage) and the subsequent damage annealing study in various atmospheres [39,41,42]. On the one hand, the influence of strain relaxation effect on lattice distortion has been ascertained and, on the other hand, the beneficial effect for the damage recovery of using wet oxygen annealing has been shown. This is, then, a clear route for further work in order to try to improve the optical quality of the LT waveguides produced by SHI irradiation.

Optics EXPRESS

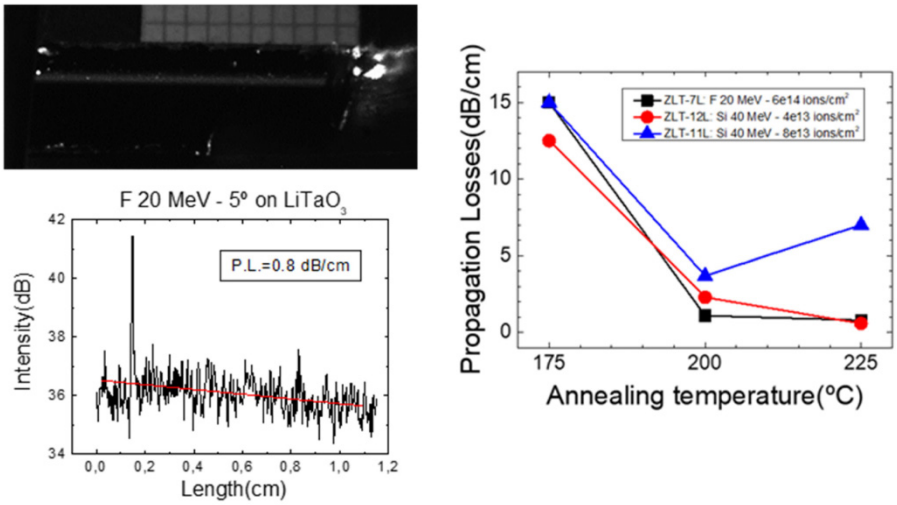

Fig. 8. Propagation losses (for the ordinary polarization, at λ = 632.8 nm) versus annealing temperature for some of the waveguides fabricated in LiTaO3 by Fluorine and Silicon irradiation.

8. Conclusions

We have performed a detailed study of successful optical waveguide fabrication in $LiTaO_3$ by SHI irradiation with C, F and Si ions in the energy range of 15 - 40 MeV. The irradiations have been chosen to be in the subthreshold amorphization regime, that requires significant ion tracks overlap to create the necessary accumulated damage. We have found an interesting scenario were the initial damage kinetics is of nuclear type and, then, for higher fluences it clearly evolves to include some type of synergy between the nuclear and electronic excitation. The refractive index profiles have been systematically characterized by dark mode analysis and in situ optical reflectance measurements. The structural disorder depth profiles of the waveguides has been ascertained by RBS/channeling. Low optical propagation losses below 0.5 dB/cm have been obtained for suitable annealing conditions. The thermal-spike model scenario has been discussed to be adequate to explain the rough electronic damage rate generation, by comparing the results from this work on LiTaO3 with the available data from the reference $LiNbO_3$.

Funding

Ministerio de Economía y Competitividad (MAT-2011-28379-C03-02 and MAT2014-577040C3-1-R); Comunidad de Madrid [Program TECHNOFUSION(II)-CM(S2013/MAE-2745).

Acknowledgements

V. Tormo-Márquez thanks the CMAM-UAM for their financial support. We thank the Technical staff of the CMAM-UAM center for support with the ion irradiations.

References

1. T. Volk and M. Wöhlecke, "Lithium Niobate, Defects, Photorefraction and Ferroelectric Switching", Springer Series in Materials Science 115, (Springer-Verlag, Berlin 2008).
2. P. Günter, "Nonlinear Optical Effects and Materials", Springer Series in Optical Science, Vol. 72, (Berlin Heidelberg New York, 2000).
3. G. L. Tangonan, M. K. Barnoski, J. F. Lotspeich, and A. Lee, "High optical power capabilities of Ti-diffused $LiTaO_3$ waveguide modulator structures," Appl. Phys. Lett. **30**(5), 238–239 (1977).
4. I. Dolev, A. Ganany-Padowicz, O. Gayer, A. Arie, J. Mangin, and G. Gadret, "Linear and nonlinear optical properties of MgO: $LiTaO_3$," Appl. Phys. B **96**(2-3), 423–432 (2009).

Optics EXPRESS

5. Y. Kondo, and Y. Fujii, "Temperature Dependence of the Photorefractive Effect in Proton-Exchanged Optical Waveguides Formed on Lithium Tantalate Crystals", Jpn. J. Appl. Phys. 34 (Part 2, No. 3B), 365–367 (1995).
6. K. Kitamura, Y. Furukawa, K. Niwa, V. Gopalan, and T. E. Mitchell, "Crystal growth and low coercive field 180° domain switching characteristics of stoichiometric $LiTaO_3$," Appl. Phys. Lett. **73**(21), 3073–3075 (1998).
7. K. Mizuuchi, K. Yamamoto, and M. Kato, "Generation of ultraviolet light by frequency doubling of a red laser diode in a first-order periodically poled bulk $LiTaO_3$," Appl. Phys. Lett. **70**(10), 1201–1203 (1997).
8. V. Ya. Shur, E. V. Nikolaeva, E. I. Shishkin, V. L. Kozhevnikov, A. P. Chernykh, K. Terabe, and K. Kitamura, "Polarization Reversal in Congruent and Stoichiometric Lithium Tantalate," Appl. Phys. Lett. **79**(19), 3146–3148 (2001).
9. V. Ya. Shur, A. R. Akhmatkhanov, M. A. Chuvakova, and I. S. Baturin, "Polarization Reversal and Domain Kinetics in Magnesium Doped Stoichiometric Lithium Tantalate," Appl. Phys. Lett. **105**(15), 152905 (2014).
10. M. Marangoni, M. Lobino, R. Ramponi, E. Cianci, and V. Foglietti, "High quality buried waveguides in stoichiometric $LiTaO_3$ for nonlinear frequency conversion," Opt. Express **14**(1), 248–253 (2006).
11. A. C. Busacca, E. D'Asaro, A. Pasquazi, S. Stivala, and G. Assanto, "Ultraviolet generation in periodically poled lithium tantalate waveguides," Appl. Phys. Lett. **93**(12), 121117 (2008).
12. P. D. Townsend, P. J. Chandler, and L. Zhang, "Optical effects of ion implantation". Cambridge University Press (1994).
13. E. Glavas, L. Zhang, P. J. Chandler, and P. D. Townsend, "Thermal stability of ion-implanted $LiTaO_3$ and $LiNbO_3$ optical waveguides," Nucl. Instr. and Meth. in Phys. Res. B **32**(1–4), 45–50 (1988).
14. V. V. Atuchin, "Causes of refractive indices changes in He-implanted LiNbO3 and $LiTaO_3$ waveguides," Nucl. Instr. and Meth. in Phys. Res. B **168**, 498–502 (2000).
15. C. Mingotte, "Proton and helium implanted waveguides in pure and Nd-doped lithium tantalate," Nucl. Instr. and Meth. in Phys. Res. B **229**, 55–59 (2005).
16. L. Jentjens, K. Peithmann, K. Maier, H. Steigerwald, and T. Jungk, "Radiation-damage-assisted ferroelectric domain structuring in magnesium-doped lithium niobate," Appl. Phys. B **95**(3), 441–445 (2009).
17. M. Lilienblum, A. Ofan, A. Hoffmann, O. Gaathon, L. Vanamurthy, S. Bakhru, H. Bakhru, R. M. Osgood, Jr., and E. Soergel, "Low-voltage nanodomain writing in He-implanted lithium niobate crystals," Appl. Phys. Lett. **96**(8), 082902 (2010).
18. A. Ofan, M. Lilienblum, O. Gaathon, A. Sehrbrock, A. Hoffmann, S. Bakhru, H. Bakhru, S. Irsen, R. M. Osgood, Jr., and E. Soergel, "Large-area regular nanodomain patterning in He-irradiated lithium niobate crystals," Nanotechnology **22**(28), 285309 (2011).
19. J. Olivares, G. García, A. García-Navarro, F. Agulló-López, O. Caballero, and A. García-Cabañes, "Generation of high confinement step-like optical waveguides in $LiNbO_3$ by swift heavy ion beam irradiation," Appl. Phys. Lett. **86**(86), 183501 (2005).
20. M. Jubera, J. Villarroel, A. García-Cabañes, M. Carrascosa, J. Olivares, F. Agullo-López, A. Méndez, and J. B. Ramiro, "Analysis and optimization of propagation losses in $LiNbO_3$ optical waveguides produced by swift heavy-ion irradiation," Appl. Phys. B **107**(1), 157–162 (2012).
21. J. Olivares, A. García-Navarro, G. García, A. Méndez, F. Agulló-López, A. García-Cabañes, M. Carrascosa, and O. Caballero, "Nonlinear optical waveguides generated in lithium niobate by swift-ion irradiation at ultralow fluences," Opt. Lett. **32**(17), 2587–2589 (2007).
22. A. García-Navarro, J. Olivares, G. García, F. Agulló-López, S. García-Blanco, C. Merchant, and J. S. Aitchison, "Fabrication of optical waveguides in KGW by swift heavy ion beam irradiation," Nucl. Instrum. Method B **249**(1-2), 177–180 (2006).
23. J. Manzano-Santamaría, J. Olivares, A. Rivera, and F. Agulló-López, "Electronic damage in quartz (c-SiO2) by MeV ion irradiations: Potentiality for optical waveguiding applications," Nucl. Instrum. Methods B. **272**, 271–274 (2012).
24. A. Majkić, M. Koechlin, G. Poberaj, and P. Günter, "Optical microring resonators in fluorineimplanted lithium niobate," Opt. Express **16**(12), 8769–8779 (2008).
25. M. Jubera, A. García-Cabañes, J. Olivares, A. Alcázar, and M. Carrascosa, "Particle trapping and structuring on the surface of $LiNbO_3$:Fe optical waveguides using photovoltaic fields," Opt. Lett. **39**(3), 649–652 (2014).
26. O. Caballero-Calero, A. García-Cabañes, M. Carrascosa, F. Agulló-López, J. Villarroel, M. Crespillo, and J. Olivares, "Periodic poling of optical waveguides produced by swift-heavy ion irradiation in $LiNbO_3$," Appl. Phys. B **95**(3), 435–439 (2009).
27. J. Olivares, M. L. Crespillo, O. Caballero-Calero, M. D. Ynsa, A. García-Cabañes, M. Toulemonde, C. Trautmann, and F. Agulló-López, "Thick optical waveguides in lithium niobate induced by swift heavy ions (~10 MeV/amu) at ultralow fluences," Opt. Express **17**(26), 24175–24182 (2009).
28. F. Chen, "Photonic guiding structures in lithium niobate crystals produced by energetic ion beams," J. Appl. Phys. **106**(8), 081101 (2009).
29. M. Toulemonde, W. Assmann, C. Dufour, A. Meftah, and C. Trautmann, "Nanometric transformation of the matter by short and intense electronic excitation: Experimental data versus inelastic thermal spike model," Nucl. Instr. and Meth. in Phys. Res. B **277**, 28–39 (2012).
30. F. Agulló-López, A. Climent-Font, Á. Muñoz-Martín, J. Olivares, and A. Zucchiatti, "Ion beam modification of dielectric materials in the electronic excitation regime: cumulative and exciton models," Prog. Mater. Sci. **76**, 1–58 (2016).

Optics EXPRESS

31. G. Fu, X. Qin, and X. Wang, ""Optical waveguide formed in a $LiTaO_3$ crystal by using MeV C3+ ion implantation", Journ. of the Kor. Phys," Society **56**(4), 1364–1368 (2010).
32. G. Liu, R. He, S. Akhmadaliev, J. R. Vázquez de Aldana, S. Zhou, and F. Chen, "Optical waveguides in $LiTaO_3$ crystals fabricated by swift $C5^+$ ion irradiation," Nucl. Instr. and Meth. in Phys. Res. B **325**, 43–46 (2014).
33. P. Liu, Q. Huang, T. Liu, S. S. Guo, L. Zhang, Y. F. Zhou, and X. L. Wang, "Visible and near-infrared waveguide properties in $LiTaO_3$ crystal produced by swift Ar 8+ ion irradiation," Appl. Phys. B **108**(3), 675–681 (2012).
34. Center of Micro-analysis of Materials, www.cmam.uam.es
35. G. Szenes, "General features of latent track formation in magnetic insulators irradiated with swift heavy ions," Phys. Rev. B Condens. Matter **51**(13), 8026–8029 (1995).
36. The Stopping and Ranges of Ions in Solids, edited by J.F. Ziegler, J.P. Biersack and U. Littmark (Pergamon Press, New York, 1985); see also www.srim.org
37. K. S. Chiang, "Construction of refractive-index profiles of planar dielectric waveguides from the distribution of effective indexes," J. Lightwave Technol. **3**(2), 385–391 (1985).
38. O. Peña-Rodríguez, M. L. Crespillo, P. Díaz-Nuñez, J. M. Perlado, A. Rivera, and J. Olivares, "In situ monitoring the optical properties of dielectric materials during ion irradiation," Opt. Mater. **6**(3), 734–742 (2016).
39. Z. Zhang, I. A. Rusakova, and W. K. Chu, "Amorphization and annealing of LiTaO3 single crystal irradiated with Ar+ ions at 77 K," J. Appl. Phys. **91**(6), 3562–3568 (2002).
40. N. Sellami, M. L. Crespillo, Y. Zhang, and W. J. Weber, "Two-stage synergy of electronic energy loss with defects in $LiTaO_3$ under ion irradiation," Mater. Res. Lett. **6**(6), 339–344 (2018).
41. Z. Zhang, I. A. Rusakova, J. Wilson, R. Chu, and W. K. Chu, "Thermal annealing of Ar ion bombarded lithium tantalate ($LiTaO_3$) single crystal," Nucl. Instr. and Meth. in Phys. Res. B **127-128**, 515–519 (1997).
42. Z. Zhang, I. A. Rusakova, and W. K. Chu, "Preservation of original single domain phase in the implanted $LiTaO_3$ single crystal by using hot implantation," Jpn. J. Appl. Phys. **38**(7), 740–742 (1999).